Author/s:
Roelli, MA;Ruffieux-Daidié, D;Stooss, A;ElMokh, O;Phillips, WA;Dettmer, MS;Charles, RP

Title:
PIK3CAH1047R-induced paradoxical ERK activation results in resistance to BRAFV600E specific inhibitors in BRAFV600E PIK3CAH1047R double mutant thyroid tumors

Date:
2017-01-01

Citation:
Roelli, M. A., Ruffieux-Daidié, D., Stooss, A., ElMokh, O., Phillips, W. A., Dettmer, M. S. & Charles, R. P. (2017). PIK3CAH1047R-induced paradoxical ERK activation results in resistance to BRAFV600E specific inhibitors in BRAFV600E PIK3CAH1047R double mutant thyroid tumors. Oncotarget, 8 (61), pp.103207-103222. https://doi.org/10.18632/oncotarget.21732.

Persistent Link:
https://hdl.handle.net/11343/255420

www.impactjournals.com/oncotarget/ Oncotarget, 2017, Vol. 8, (No. 61), pp: 103207-103222

Research Paper

PIK3CA^{H1047R}-induced paradoxical ERK activation results in resistance to BRAF^{V600E} specific inhibitors in BRAF^{V600E} PIK3CA^{H1047R} double mutant thyroid tumors

Matthias A. Roelli[1], Dorothée Ruffieux-Daidié[1], Amandine Stooss[1], Oussama ElMokh[1], Wayne A. Phillips[3], Matthias S. Dettmer[2] and Roch-Philippe Charles[1]

[1]Institut für Biochemie und Molekulare Medizin, Universität Bern, Bern, Switzerland

[2]Institut für Pathologie, Universität Bern, Bern, Switzerland

[3]Cancer Biology Laboratory, Peter MacCallum Cancer Centre, Melbourne, Australia

Correspondence to: Roch-Philippe Charles, **email:** roch-philippe.charles@ibmm.unibe.ch

Keywords: *aggressive thyroid cancer, BRAF^{V600E} inhibitor resistance, PI3'K inhibitors, paradoxical ERK activation, overcoming resistance*

Received: *January 17, 2017* ***Accepted:*** *September 23, 2017* ***Published:*** *October 11, 2017*

ABSTRACT

Thyroid carcinomas are the most prevalent endocrine cancers. The BRAF^{V600E} mutation is found in 40% of the papillary type and 25% of the anaplastic type. BRAF^{V600E} inhibitors have shown great success in melanoma but, they have been, to date, less successful in thyroid cancer. About 50% of anaplastic thyroid carcinomas present mutations/amplification of the phosphatidylinositol 3' kinase. Here we propose to investigate if the hyper activation of that pathway could influence the response to BRAF^{V600E} specific inhibitors.

To test this, we used two mouse models of thyroid cancer. Single mutant (BRAF^{V600E}) mice responded to BRAF^{V600E}-specific inhibition (PLX-4720), while double mutant mice (BRAF^{V600E}; PIK3CA^{H1047R}) showed resistance and even signs of aggravation. This resistance was abrogated by combination with a phosphoinositide 3-kinase inhibitor. At the molecular level, we showed that this resistance was concomitant to a paradoxical activation of the MAP-Kinase pathway, which could be overturned by phosphoinositide 3-kinase inhibition *in vivo* in our mouse model and *in vitro* in human double mutant cell lines.

In conclusion, we reveal a phosphoinositide 3-kinase driven, paradoxical MAP-Kinase pathway activation as mechanism for resistance to BRAF^{V600E} specific inhibitors in a clinically relevant mouse model of thyroid cancer.

INTRODUCTION

Thyroid cancer is the most frequent form of endocrine malignancy. Papillary thyroid cancer (PTC) is the most prevalent type of thyroid carcinoma (80%). It is moderately aggressive, moderately lymphometastatic and has a response rate above 90% to standard radioiodine treatment. The main risk is a possible progression (5–10% of the cases) to more aggressive variants including radio-iodine-resistant PTC, poorly differentiated thyroid carcinoma and anaplastic thyroid carcinoma (ATC) [1]. For ATC, the survival rate is very poor with a median survival of 2–7 months after diagnosis and a mortality rate of 90% within the first year after diagnosis [2]. Metastases can be observed in 10–20% of ATC cases, mainly in the lung and bones [3]. However, unlike most cancer patients, ATC patients do not predominantly succumb to "dissemination" of the disease, but rather to local invasion of the tumor into the tracheal space. Undifferentiated cancer cells invade the space between the cartilage ring and the tracheal epithelium inducing dyspnea and suffocation [4]. The thyroid's localization next to major vessels like the carotids makes complete curative resection impossible. There is currently no efficient treatment for ATC, the disease being highly resistant to radio- and chemotherapies, including radioiodine I^{131} that usually

yields excellent therapeutic outcome in other thyroid cancers.

BRAF is part of the canonical signaling pathway RAS RAF➔MEK➔ERK hereafter termed MAPK pathway. The mutant gene coding for $BRAF^{V600E}$ is found in almost 45% of PTCs and 20–40% of ATCs, making it the most common genetic alteration in thyroid cancer (~40% overall) [5, 6]. Independent models expressing the $BRAF^{V600E}$ mutation specifically in the thyroid demonstrate that this constitutively active form of the protein leads to development of PTC [7, 8], thus confirming the importance of the mutation in pathogenesis. More recent models show that $BRAF^{V600E}$ can collaborate with p53 deletion [9] or with $PIK3CA^{H1047R}$ mutation [10] to promote PTC progression to ATC.

The phosphatidylinositol 3' kinase or PI3'K is part of the RAS PI3'K➔AKT mTOR pathway hereafter termed PI3'K pathway. PI3'K phosphorylates phosphoinositides on the 3 position of the inositol ring [11] resulting in AKT recruitment to the membrane and its phosphorylation [12]. There are several PI3'K which are heterodimers composed of a catalytic and a regulatory subunit. *PIK3CA* codes for the p110α catalytic subunit of class I PI3'K [13]. The $PIK3CA^{H1047R}$ mutation renders the protein constitutively active and can be frequently found in cancers [14]. PI3'K signaling alterations frequently occur in aggressive thyroid cancers with 40% gene amplification and 20% mutations [15, 16].

Pharmacological mutation specific inhibition of $BRAF^{V600E}$ with vemurafenib leads to a dramatic tumor regression in melanoma patients [17–19]. Unfortunately, half of the patients relapse after six months of treatment. Many routes to acquired resistance have been proposed, including elevated expression of CRAF [20] or BRAF kinases or aberrant expression of a BRAF splice variants [21–23]. All these resistance mechanisms lead to the reactivation of RAF kinases. In addition, several other means of acquired resistance are described, involving mutations in other partners of the MAPK pathway such as N-RAS [24] or MEK [25]. Remarkably, all these mechanisms result in MAPK pathway reactivation, as demonstrated by ERK phosphorylation, and eventually lead to a resumption of tumor growth. This emphasizes the central role of the MAPK pathway as the main driver of tumor growth and resistance and the necessity to pharmacologically target that pathway to achieve tumor reduction.

Even though 40% of all thyroid tumors harbor the $BRAF^{V600E}$ mutation, unlike in melanoma, it is not clear whether $BRAF^{V600E}$ inhibition could be used against thyroid tumors. About 10% or thyroid cancers are incurable because of diffuse presentation that make them inoperable as well as their loss of iodine hunger. New targeted therapies are therefore urgently needed for ATC and radio-iodine-resistant PTC. There are some encouraging results from single case studies in $BRAF^{V600E}$ positive ATC [26, 27] and also for invasive $BRAF^{V600E}$ positive PTC albeit from reports of very small cohorts [28]. The biggest study so far concerns 7 ATC patients with various responses from complete/partial regression but surprisingly also to tumor progression [29]. Overall these studies suggest an approximate 50% response rate to $BRAF^{V600E}$ inhibitors in aggressive thyroid cancer. One case even showed patient's rapid worsening which is the actual opposite of what was expected after vemurafenib treatment [27]. This suggests "pre-existing" drug resistance that does not result from treatment adaptation over a few weeks as it is the case in melanomas.

Understanding these refractory forms of cancer is essential for efficient use of targeted therapies. In this study, we used a $BRAF^{V600E}$ $PIK3CA^{H1047R}$ double mutant, as well as a $BRAF^{V600E}$ single mutant mouse model to investigate the tumor burden response to $BRAF^{V600E}$ specific inhibition. Our experiments showed that the $PIK3CA^{H1047R}$ mutation conferred resistance to the drug. This resistance was waived by combination treatment with a PI3'K inhibitor. The resistance was correlated to paradoxical hyperactivation of ERK, that was also depending on PI3'K activity.

RESULTS

$BRAF^{V600E}$ single mutant thyroid tumor respond to PLX4720 inhibition, while $BRAF^{V600E}$; $PIK3CA^{H1047R}$ double mutant tumors do not

Our primary aim was assessing the effect of $BRAF^{V600E}$ inhibition in our two mouse models. The $BRAF^{V600E}$ single, and the $BRAF^{V600E}$/$PIK3CA^{H1047R}$ double mutant. PLX-4720, a commonly used pre-clinical surrogate for vemurafenib [30–32] that is similarly potent but more soluble/bioavailable [33] was used to inhibit $BRAF^{V600E}$ specifically.

Mice were bred, tumors induced at the age of one month and the treatments started two months after tumor induction to allow tumors to form (Figure 1A), but still leave enough time to treat mice for 3 more months without reaching 6 months after induction when mice usually reach endpoint (whistling, breathing issues and consequent sudden weight loss) (Figure 1A).

In single mutant mice, the PLX-4720 drug treatment induced a significant tumor size reduction (-20%) that lasted for more than 10 weeks, while controls increased in size by more than 50% (Figure 1B). In double mutant mice, tumors were bigger and grew faster than in single mutant. The control group grew rapidly and steadily during the 10 weeks of monitoring. PLX-4720 treated animals had a modest drug response for 3 weeks (-10%), then tumor burden resumed growth at a similar rate to control mice with a tumor burden increase of +12 percentage points per week (Figure 1C and 1D). Much to our concern, 3 out of 5 animals from this group had to be removed (crosses on Figure 1C) during the course

of the experiment as they were reaching predefined endpoint criteria (see above paragraph). This worsening of the condition was only witnessed in PLX-4720 treated animals. GDC-0941 treated animals presented an initial tumor burden reduction of 20% then tumor size stabilized for the rest of the treatment period. Interestingly, when a drug combination of PLX-4720 and GDC-0941 was administered, mice showed a robust response with 60% lower tumor burden after 6 weeks followed by stabilization until the end of the experiment (Figure 1C and 1D).

Double mutant tumors present histological worsening after BRAF^{V600E} specific inhibition

After 10 weeks of treatment, 3 double mutant mice per group were dissected and their thyroids were processed for histological analysis. Control mice had the expected histology (Figure 2A): aggressive PTC with tall cell variant (Figure 2A middle), and foci presenting signs of phenotypic progression to ATC (Figure 2A bottom). GDC-0941-treated mice had smaller thyroid sections, while presenting a similar histology compared to controls (Figure 2B) with a mixture of PTC (Figure 2B middle) containing small ATC foci (Figure 2B bottom). Animals treated with the drug combination also presented smaller thyroid sections but in these PTC areas were almost absent (Figure 2C), leaving connective tissue (Figure 2C middle) and cholesterol clefts, but ATC foci remained (Figure 2C bottom).

PLX-4720-treated thyroids (Figure 2D) presented large PTC nodule areas that were more solid and featuring areas of the hobnail type of PTC (Figure 2D Middle) and large areas of ATC (Figure 2D bottom). In early terminated PLX-4720 animals (Figure 2E), while areas of PTC persist (Figure 2E middle) larger ATC areas could be found (Figure 2E Middle), invading the surrounding muscles (Figure 2E bottom), and eventually the tracheal rings. Overall, they looked more progressed than any other group. Immunostainings were preformed to confirm the pathological analysis. PTC areas were positive for galectin-3 and cytokeratin 19 while ATC areas were positive for galectin-3 and vimentin (Figure 2F).

Double mutant tumors present paradoxical activation of ERK after 10 weeks of PLX-4720 treatment

Signaling pathways in the tumors were investigated by western blot. PLX-4720-treated animals displayed an unexpected paradoxically elevated ERK1/2 phosphorylation ratio compared to the controls after 10 weeks of treatment. When treated with GDC-0941 alone, ERK1/2 phosphorylation was unchanged compared to controls. When treated with drug combination, ERK paradoxical activation was abolished resulting in ERK phosphorylation level comparable to controls. AKT phosphorylation was not affected by PLX-4720 while GDC-0941 treatment resulted in a small but significant reduction of AKT phosphorylation (Figure 3A).

For comparison, we performed western blots with proteins extracted from BRAF^{V600E} single mutant mice. In this case, after 70 days of PLX-4720 treatment, ERK phosphorylation in treated animals was comparable to the non-treated. As expected, PLX4720 treatment did not affect AKT phosphorylation significantly (Figure 3B).

Paradoxical activation of ERK also occurs after short periods of PLX-4720 treatment

To confirm the observed paradoxical ERK activation, we treated mice with the same drugs for a shorter period of 10 days. We observed the same trend for tumor burden as seen after 10 weeks (Figure 4A). Only GDC-0941 and drug combination treated animals showed tumor burden reduction. PLX-4720 treated animals displayed a tumor burden that was not statistically different from the controls but appeared elevated from the two other groups (Figure 4A).

Similarly to the observed effect at 10 weeks, after 10 days of treatment we observed paradoxical activation of ERK under PLX-4720 treatment that was abrogated by the drug combination (Figure 4B). To complete this part, we also treated double mutant animals only once with PLX-4720 or GDC-0941 and dissected the animals four hours after drug administration. At this time, the PLX-4720 driven paradoxical activation of ERK was already observable. GDC-0941 treatment on the other hand led to a pronounced de-phosphorylation of AKT.

Finally, to ensure that ERK phosphorylation signal was coming from tumor cells, we performed immunofluorescence staining on tumor samples. The signal was clearly located in the tumor cells and not in the mesenchyme or coming from infiltrating immune cells. The specificity of our staining was verified by treating mice with the potent MEK1/2 inhibitor PD-325901 [34] that completely abrogated ERK phosphorylation after 10 consecutive days of treatment (Figure 4C).

Drug combination induces increased cell death *in vivo*

Searching for the mechanisms driving the observed tumor reduction, we performed immunofluorescence staining for Ki67. We could only detect a significant increase of Ki67 index in PLX-4720 treated animals compared to the drug combination group (Figure 5A). Then we performed TUNEL staining to monitor DNA fragmentation. The count of apoptotic bodies was increased in GDC-0941 and drug combination treatment (Figure 5B). In addition, we detected a reduced count in PLX-4720 treated tumors. We then performed a Masson's trichrome staining to evidence collagen accumulation

stained in blue (Figure 5C). Interestingly, the drug combination treatment led to a significantly increased proportion of collagen rich areas inside the thyroid lobes, evidencing higher tumor regression. Tumors from PLX-4720-treated mice had a significantly lower proportion of collagen in the tumor tissue.

Paradoxical activation of ERK under BRAF^{V600E} specific inhibition treatment is also PI3'K-dependent in human ATC cell lines

To further demonstrate that paradoxical activation of ERK also depends on PI3'K signal in human ATC cells,

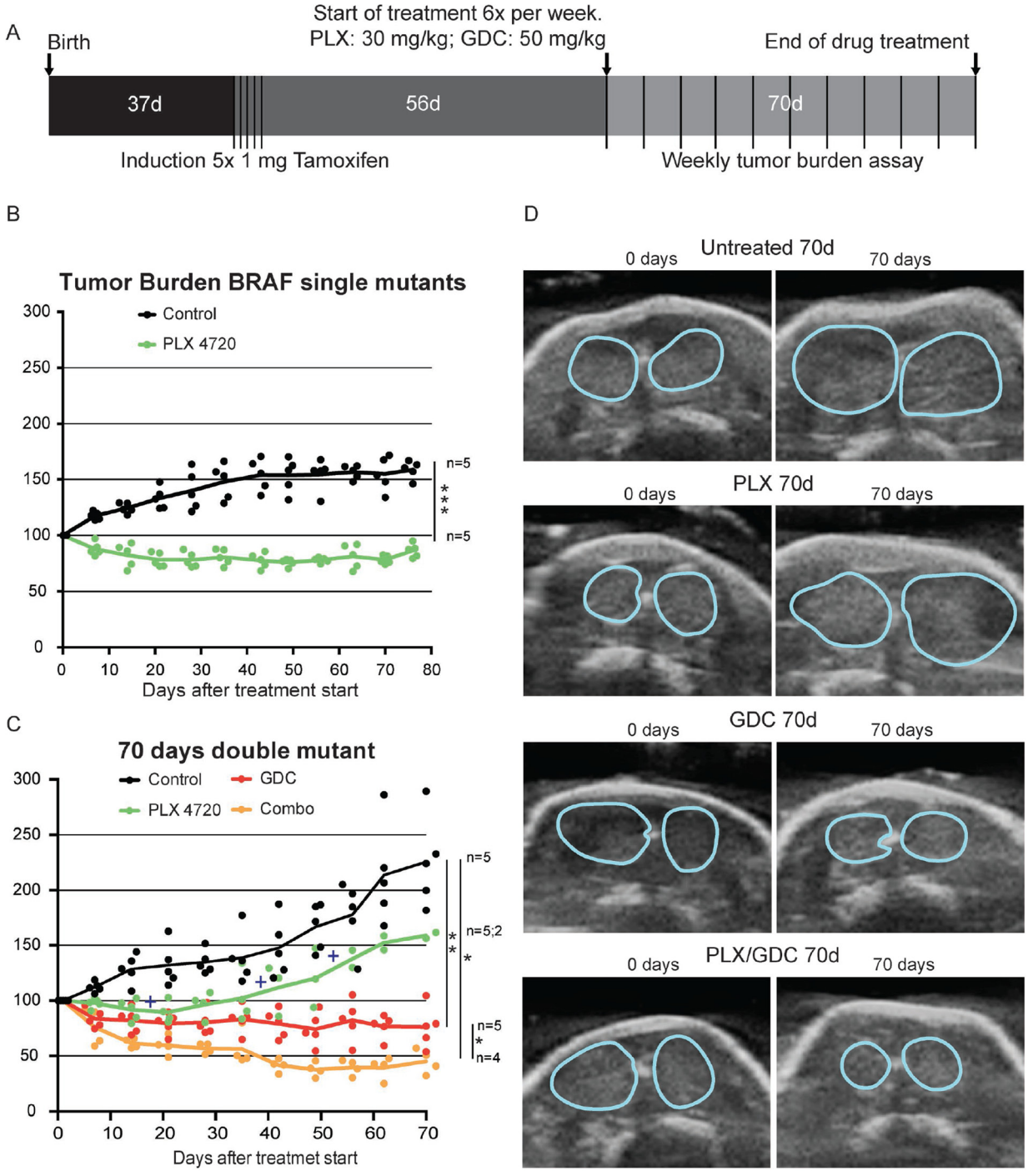

Figure 1: PI3'K inhibition counteracts PLX-4720 resistance in a double mutant thyroid cancer mouse model. (**A**) Schematic timeline depiction of *in vivo* Experiment. Tumor burden in single mutant *Braf*$^{CA/+}$*; ThyroglobulinCre*^{ERT2} mice (**B**) and double mutant *Braf*$^{CA/+}$*; Pik3ca*$^{Lat/+}$; *ThyroglobulinCre*^{ERT2} mice (**C**) in percentage of the tumor burden at the beginning of the drug treatment. Crosses represent events of mice reaching end-point criteria. (**D**) Representative pictures from ultrasound imaging of double mutant mice after 70 days of treatment used for assessment of the tumor burden. Thyroid outlines are shown by blue lines.

we used three cell lines. OCUT-2 cells harbor the same mutations as the double mutant mouse model ($BRAF^{V600E}$/$PIK3CA^{H1047R}$), whereas 8505c and SW1736, analogous to the single mutant mice, only have the $BRAF^{V600E}$ mutation. The mutational status of *PIK3CA* in these cell lines was confirmed by sequencing [35]. As paradoxical ERK activation has been described to be dependent on drug concentration [36], we exposed the cells to decreasing concentrations of PLX-4032 (vemurafenib). Interestingly, OCUT-2 cells had a greater than 2-fold increase in p-ERK/

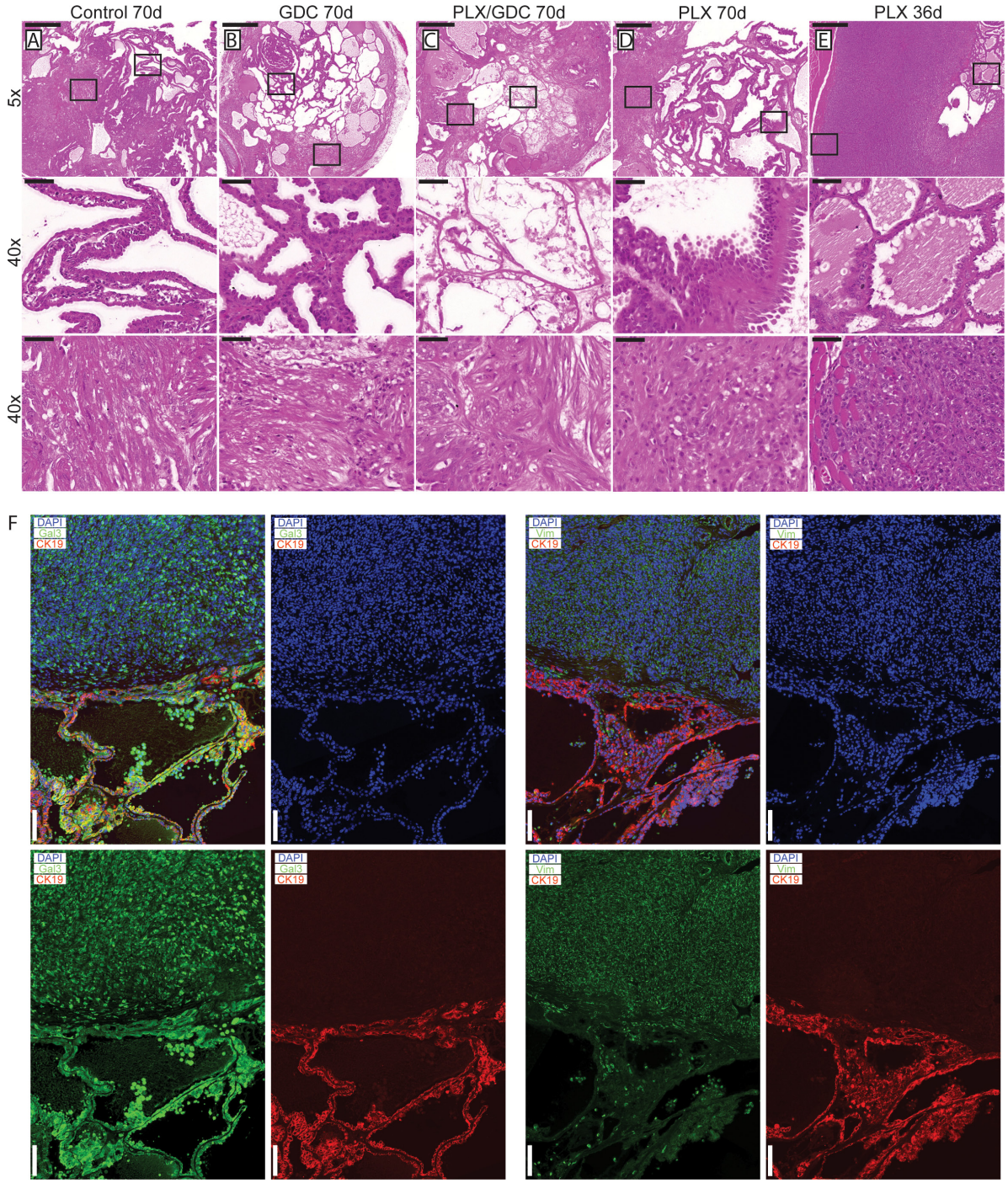

Figure 2: Histological presentation of tumors after 70 days of drug treatments. H & E staining from formalin fixed paraffin embedded and sectioned (5 µm) thyroids from double mutant mice after 70 days of treatment. Representative thyroid tissues at the end of the treatment of (**A**) control, (**B**) 50 mg/kg GDC-0941, (**C**) drug combination (50 mg/kg GDC-0941 and 30 mg/kg PLX-4720 and (**D**) 30 mg/kg PLX-4720 treated mice. (**E**) H and E staining of thyroid tissues from a double mutant mouse treated with PLX-4720 reaching endpoint after 36 days of treatment. Scale bars: 500 µm (upper panels) 50 µm (middle and lower panels). (**F**) Immunostainings of representative PTC and ATC tissues stained for Cytokeratin 19 (red) DAPI/nuclei (blue) and either Galectin-3 or Vimentin (green). Scale bars 100 µm.

tot-ERK ratio compared to vehicle treated cells, at low concentrations: 1.6 and 8 nM (Figure 6A). Paradoxical ERK hyper-phosphorylation was not detectable when cells were subjected to GDC-0941 in addition to PLX-4032 drug dilutions. When we treated them with the same concentrations of PLX-4032, 8505c and SW1736 cells did not exhibit paradoxical ERK activation (Figure 6B). The additional treatment with GDC-0941 did not affect either the baseline ERK phosphorylation or the response to PLX-4032 regardless of the PLX-4032 concentration in 8505c cells. To strengthen this point, we have also performed a similar experiment using BKM-120, another PI3'K inhibitor (Supplementary Figure 1). In this case, BKM-120 similarly abrogated the paradoxical effect seen in OCUT-2, demonstrating that the phenomenon observed is unlikely to be caused by a possible off-target effect of GDC-0941 but was rather specific to its inhibitory effect on PI3'K activity.

DISCUSSION

The $BRAF^{V600E}$ mutation is detected in many cancer types such as melanoma, colon, ovarian, lung and prostate cancers [37, 38]. In general, it accounts for 8% of all mutations in human cancers [37]. The development of specific inhibitors against this mutation has raised a lot of interest in the clinics, for its potential lack of side effects. There is a strong rational to translate the success of vemurafenib from melanoma to other $BRAF^{V600E}$ positive tumors like PTC or ATC. Unfortunately, case studies using vemurafenib in aggressive invasive-PTC and ATC show diverse results ranging from regression to no response or even aggravation [26–29].

We showed here that $BRAF^{V600E}$ inhibition presented the expected response in $BRAF^{V600E}$ single mutant mice (Figure 1B). Tumor burden decreased at first then reached a plateau, reflecting the fact that after an initial response phase, MAPK signaling is transduced through $BRAF^{WT}$ restoring a "normal" level of ERK phosphorylation (Figure 3B) resulting in no further clinical benefit of the drug. This was rather expected. On the other hand, when subjected to the same dose of PLX-4720, $BRAF^{V600E}$ $PIK3CA^{H1047R}$ double mutant tumors regrew after a very short initial response (Figure 1C). This suggests that the additional $PIK3CA^{H1047R}$ mutation resulted in a rapid resistance to $BRAF^{V600E}$ specific inhibition. This was confirmed by the resistance break obtained by the inhibition of PI3'K activity with the addition of GDC-0941 to the treatment regime. Consistently, recent studies in a model of colorectal cancer have shown that resistance to PLX-4720 treatment *in vivo* can be relieved by inhibition of PI3'K [39].

The initial phase of tumor reduction after PLX-4720 treatment in the double mutant model can be explained by tumor heterogeneity. Indeed, in this mouse model, tumors consist of rare normal follicles amongst large PTC and ATC foci (Figure 2A–2E). Full Cre-driven recombination of both alleles from latent to mutant might not have occurred in every original cell. A portion of the tumors might be $BRAF^{V600E}$-single mutant and still be responsive to PLX-4720. Interestingly, in the second double mutant cohort of mice, the resistance to PLX-4720 was already detectable after 10 days of treatment most likely due to a smaller proportion of single mutant cells. GDC-0941 and drug combination on the other hand already displayed a significantly tumor reduction effect (Figure 4A),

Even though treatment with GDC-0941 clearly induced a 20% reduction in the size of the tumor (Figure 1C), possibly due to apoptosis elevation

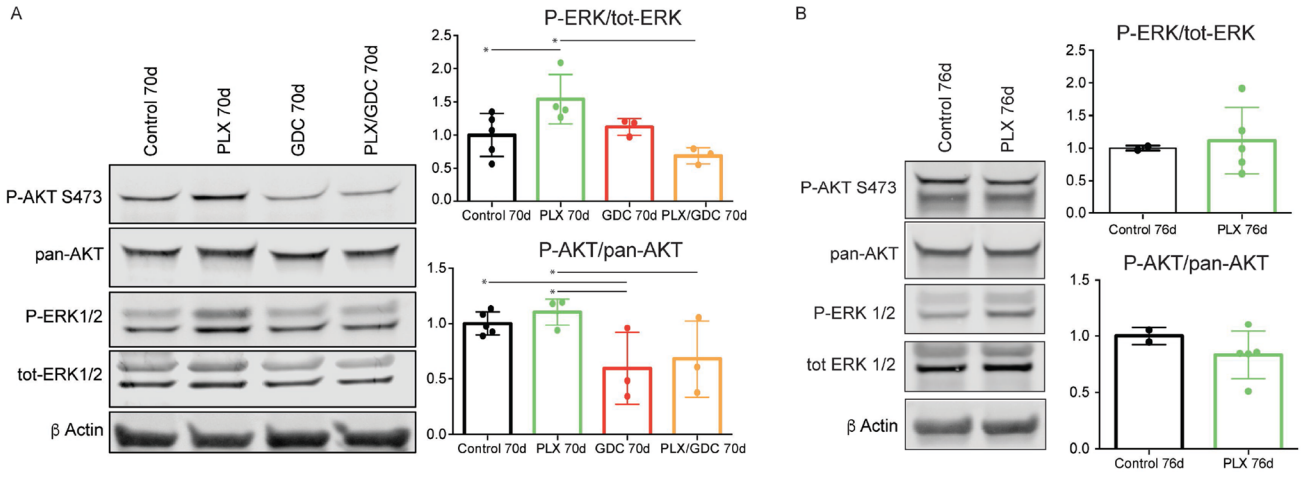

Figure 3: $BRAF^{V600E}$ and $PIK3CA^{H1047R}$ tumors present a paradoxical activation of ERK under PLX-4720 treatment after 10 weeks. (**A**) Representative pooled western blot (left), and quantification of single sample blots (right) of proteins from $BRAF^{V600E}$/$PIK3CA^{H1047R}$ double mutant mice treated for 70 days with either vehicle, PLX-4720 (30 mg/kg), GDC-0941 (50 mg/kg) or a combination of both. (**B**) Representative pooled western blot (left), and quantification of single sample blots (right) of proteins from $BRAF^{V600E}$ single mutant mice treated for 76 days with either vehicle or PLX-4720 (30 mg/kg). Error bars represent standard deviation. Values represent means of calculated ratios. Points represent single ratio values.

(Figure 5B and 5C), there was no clear beneficial effect in terms of histology (Figure 2B). In terms of pathways activation, AKT phosphorylation level was reduced profoundly after 4 hours (Figure 4B) but the effect seemed weaker after 10 days (Figure 4B) and 10 weeks (Figure 3A) of treatment. This suggests that there are mechanisms of adaptation in this pathway as well, allowing restoration of AKT phosphorylation even when PI3'K is inhibited. The fact, that there is still a cytostatic effect when treating with GDC-0941, even though AKT phosphorylation level has partially recovered, demonstrates that AKT phosphorylation and PI3'K activity/mutation are not necessarily linked in this context [40]. This suggests, that a mechanism downstream of PI3'K that does not necessarily involve AKT could be responsible for tumor promotion. These findings are consistent with a recent publication from our group were PI3'K inhibition was combined with the MEK inhibitor PD-325901 [35].

Our most unexpected observation was that double mutant mice treated with PLX-4720 alone displayed a strong increase in ERK phosphorylation (Figure 3A) after 10 weeks, that goes beyond recovery of ERK signaling that was also observed 10 days and 4 hours after treatment (Figure 4B). We confirmed this by immunofluorescence staining, where PLX-4720 treatment triggered an increase in the P-ERK signal in tumor cells (Figure 4C). $BRAF^{V600E}$ specific inhibition has been showed before to decrease P-ERK1/2 at first, then ERK activity will be restored by releasing the feedback inhibition loop between ERK and RAS, allowing "normal" RAF signaling through the wild-type allele of BRAF, as shown in our single mutant mice (Figure 3B). The over-activation that we observe in the context of our PLX-4720 treated double mutant mice is however more reminiscent of the "paradoxical effect" of RAF inhibitors [41]. This paradoxical effect was described in melanoma patients treated with vemurafenib who developed squamous cell carcinoma [42] and explained by aberrant dimerization and enhanced signaling through $BRAF^{WT}$ and CRAF. [43–46] Interestingly, this effect has been suggested to be used beneficially in wound healing [47].

The elevated ERK activation in the present study explained the worsening of the condition of the double mutant mice treated with PLX-4720 (Figure 2E). Interestingly, in order to take place, paradoxical ERK activation requires an activating signal upstream of CRAF. In this case, CRAF (also called Raf-1) could be activated by PI3'K [48]. Paradoxical ERK activation is most likely also the cause for the observed elevation of Ki67 in the tumors of PLX-4720 treated double mutant animals (Figure 5A). The elevation of the Ki67 index could also be caused by the observed ATC progression of the tumors of PLX-4720 treated animals, since ATC presents a dramatically elevated proliferation index compared to well differentiated thyroid cancers. The progression to ATC is furthermore evidenced by the decreased TUNEL (Figure 5B) and decreased collagen deposition (Figure 5C) since ATC are refractory to drug-induced apoptosis. One could speculate that a paradoxical ERK activation might also have been responsible for tumor progression in a reported case of rapid tumor progression observed when an ATC patient was treated with vemurafenib [27].

To assess whether this paradoxical ERK hyperactivation was transcriptionally regulated, we treated tumor-bearing mice with one dose of PLX-4720 and dissected tumors 4 hours post treatment. The paradoxical effect could already be observed at that point (Figure 4B and 4C) advocating for a non-transcriptionally regulated effect. Altogether this data suggests that paradoxical ERK activation is non-transcriptionally regulated and PI3'K dependent.

In vitro, the paradoxical effect was only observed in the OCUT-2 cell line (Figure 6A) that has the same mutation pattern as the double mutant $BRAF^{V600E}$/$PIK3CA^{H1047R}$ mice but not in 8505c or SW1736 cells, (Figure 6B) that have no

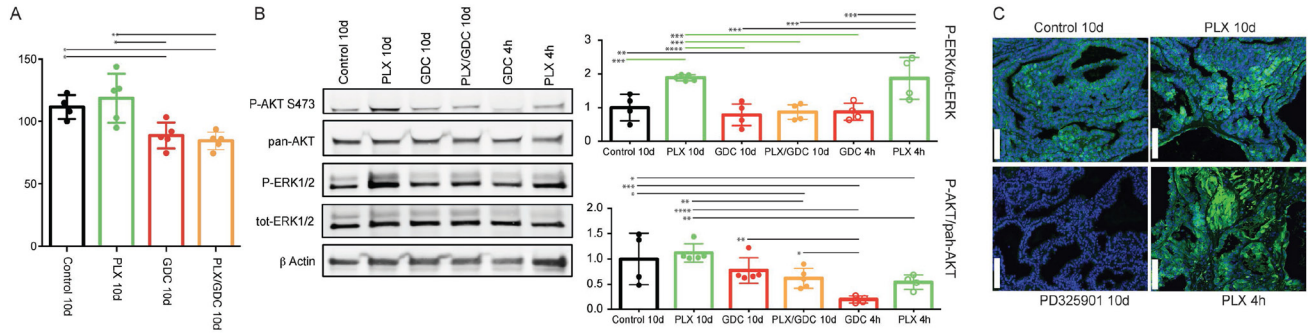

Figure 4: $BRAF^{V600E}$ and $PIK3CA^{H1047R}$ tumors present a paradoxical activation of ERK under PLX-4720 treatment also after 10 days. (**A**) Tumor burden quantification from $BRAF^{V600E}$/$PIK3CA^{H1047R}$ double mutant mice treated for 10 days with either vehicle, PLX-4720 (30 mg/kg), GDC-0941 (50 mg/kg) or a combination of both, (**B**) Representative pooled western blot (left), and quantification of single sample blots (right) of proteins from the same animals and from animals treated only once with either PLX-4720 (30 mg/kg), GDC-0941 (50 mg/kg) and dissected 4 hours later. (**C**) Immunofluorescence staining for P-ERK of formalin fixed, paraffin embedded thyroid tumor samples sectioned to 5µm from $BRAF^{V600E}$, $PIK3CA^{H1047R}$ double mutant mice treated with either vehicle, PLX-4720 (30 mg/kg or PD-325901 (5 mg/kg) for 10 days or PLX-4720 (30 mg/kg) for 4 hours. Scale bars: 100 µm.

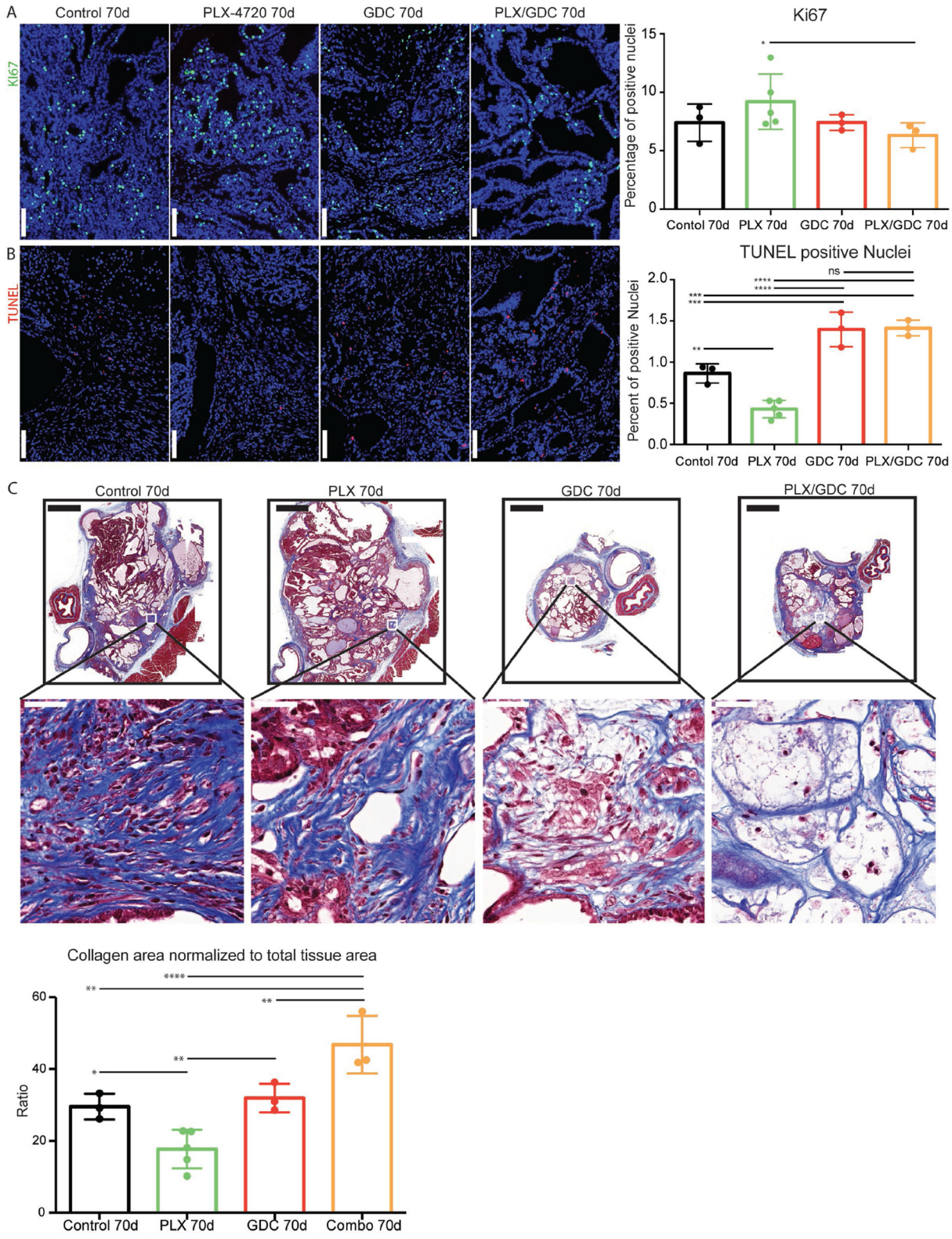

Figure 5: Drug combination induces increased cell death *in vivo*. Ki67 staining formalin fixed, paraffin embedded 5 µm tumor samples (**A**) Left side: Representative immunofluorescence after 70 days of treatment. DAPI (blue) Ki67 (green). Scale Bars: 100 µm. Right side: Quantification on whole tumors averaged from 4 consecutive sections. (**B**) Left side: TUNEL staining revealed with streptavidin-Alexa633 fluorescent probe (purple) and DAPI (blue). Scale Bars: 100 µm. Right side: TUNEL positive nuclei normalized to total nuclei counts. Scale bars: 100 µm. (**C**) Top: Representative images of Masson's trichrome stained tumor sections and higher magnifications thereof below. Scale bars: 1 mm (upper) and 50 µm (lower). Bottom: evaluation of collagen rich area normalized to total tissue area per tumor. Error bars represent standard deviation. Values represent means of calculated ratios. Points represent single ratio values.

reported alteration in PI3'K. The latter cell lines represent the single mutant mice, that did not show venurafenib induced paradoxical activation either. Consistently, 8505c used in an orthotropic xenograft model were responding to PLX-4720 treatment *in vivo* [49]. The observed effect of paradoxical ERK activation in OCUT-2 cells could again be prevented when cells were concomitantly treated with GDC-0941 (Figure 6A), once more showing that paradoxical ERK hyper-activation is dependent on PI3'K activity. It is important to note that the paradoxical effect is dependent on drug concentration and might therefore have been missed in several studies using 1 μM PLX-4032. This can be explained by the fact that at this concentration, PLX-4032 inhibits all RAF isoforms and therefore also blocks CRAF, which is required for paradoxical activation.

Drug combination treatment presented the strongest effect on tumor burden (Figure 1C). Looking at TUNEL staining, GDC-0941 and drug combination treated animals could not be distinguished (Figure 5B). Apoptosis is a short-term process of programmed cell death. In general, cell debris disappears by extracellular enzyme digestion and leukocyte phagocytosis and is replaced by accumulation of fibrotic tissue. This is measured in daily clinical practice as response to chemotherapy in so-called regression scores in various human tumor types [50–52]. Deposition of fibrotic tissue was measured by Masson's trichrome staining (Figure 5C). Masson's Trichrome staining showed significantly less deposition of fibrotic tissue in GDC-0941 treated animals, compared to combination treated animals. This revealed a slightly increased rate of cellular death in combination treated, compared to GDC-0941 treated animals that could only be visualized by a method that measures the accumulative effect of cell death. Whether this was due to apoptosis, necrosis or a different type of cell death remains unclear. With a similar Ki67 index, and TUNEL count (Figure 5), a further cell death mechanism might be involved under combination treatment (e.g. necrosis). It is also important to note that the areas that were mainly affected consisted of PTC, as demonstrated by the absence of PTC in tumors of combination treated animals. ATC foci remained (Figure 2C), meaning that this drug combination was mostly effective on PTC, but the effect on ATC remains elusive and would require more work *in vivo*.

Our data led us to propose the following mechanism for PLX-4720-induced ERK paradoxical activation and therefore resistance: $BRAF^{V600E}$ specific inhibition leads to an increased formation of an active B/CRAF heterodimer and the complex is further stimulated by PI3'K [43–46, 48, 53] resulting in increased ERK phosphorylation as schematically presented in Figure 7. The two events, stabilization of a $BRAF^{V600E}$/CRAF complex by $BRAF^{V600E}$ specific inhibitors and activation of CRAF through PI3'K, are required to obtain paradoxically hyper-phosphorylated ERK1/2 that led to the worsening of the phenotype (Figure 1). Our data are consistent with the fact that RAS activates PI3'K, and that newly arising skin tumors in vemurafenib treated $BRAF^{V600E}$ mutant melanoma patients often carry activating mutations in RAS [42]. This novel *in vivo* mechanism of resistance clearly differs from published resistance mechanisms in melanoma, where resistance seems to be acquired during the course of treatment [20, 21, 23]. Such treatment-induced adaptive mechanism was also described in the context of thyroid cancer were thyroid cancer cells show resistance to vemurafenib that was induced by up-regulation and activation of HER-3 [54]. Our data, thus, uncover a novel mechanism of vemurafenib resistance.

Regardless of the paradoxical resistance, while being beneficial, $BRAF^{V600E}$ inhibition shows some limits, since profound ERK inhibition cannot be maintained even in combination with GDC-0941. MEK1/2 inhibition is able to produce a sustained and deep MAPK inhibition in thyroid [55]. But unlike vemurafenib the toxicity of MEK inhibition does not allow long periods of treatment. The option to combine both inhibitors to achieve lower toxicity might become the standard care in melanoma [56]. But another approach is to alternate cycles of vemurafenib and drug vacancy to perturb the adaptive signaling to $BRAF^{V600E}$ inhibition [57].

Finally, our findings suggest that selecting patients for targeted therapies based on their BRAF mutational status alone is not sufficient for choosing a successful therapy. The mutational status of *PIK3CA* should also be assessed, as treating $BRAF^{V600E}$ positive patients carrying activating PI3'K mutations with $BRAF^{V600E}$-specific inhibitors may lead to ERK hyper-activation and disease aggravation. Gene amplification measurements should also be considered, since more patients seem to be resistant to vemurafenib than suggested by the PI3'K activating mutation frequency alone. In conclusion, we suggest an explanation for the observed high rate of *a priori* drug-resistance to $BRAF^{V600E}$ specific inhibitors seen in thyroid cancer. Nevertheless, we show that treating patients with $BRAF^{V600E}$ inhibitors such as vemurafenib could be a valid approach in the appropriate clinical setting including prior mutational testing of the tumor and, if applicable, administered alone or combined with PI3'K inhibitors. The combination of both PI3'K and $BRAF^{V600E}$ inhibition may lead to a stronger response and should therefore be considered in the clinics, since a clear collaborative effect is visible *in vivo*. On the other hand, the coming of the new generation of paradox-evading RAF inhibitors [58] might waive the resistance mechanism that we described here and open the way to a broader use of RAF inhibitors in the context of aggressive inoperable PTC, and ATC.

MATERIALS AND METHODS

Cell lines

The $BRAF^{V600E}$ mutant ATC cell lines 8505c and SW1736 were purchased at the Public Health England

repository and cultured in RPMI-1640, 10% FCS, 2 mM L-glutamine, MEM NEAA (Thermo Fisher) 1:100 and P/S (100U Penicilin/ml and 0.1mg Streptomycin/ml). The ATC cell line OCUT-2 carries concomitant $BRAF^{V600E}$ and $PIK3CA^{H1047R}$ mutations [59]. It was kindly provided by Prof. James Fagin (Memorial Sloan Kettering Cancer Center), validated by our group by STR profiling (Microsynth, Switzerland), and cultured in DMEM medium 10% FCS, 2 mM L-glutamine, MEM NEAA (Thermo Fisher) 1:100 and P/S (100U Penicilin/ml and 0.1mg Streptomycin/ml). The mutational status for *PIK3CA* of all three cell lines was validated by sequencing. All cell lines were cultured for a maximum of 40 passages or 6 months; whichever limit was reached first.

Drugs used

PLX-4720, PLX-4032 (vemurafenib), GDC-0941, PD-0325901 and BKM-120 were purchased from Abmole Bioscience, Hong-Kong.

Mice

All mouse experiments were performed in compliance with Swiss federal legislation and licensed by the Kanton of Bern. License Nr: BE120–13. Mice were kept in isolated ventilated cages, fed ad libitum in a 12/12 hours cycle of light and dark.

Drug administration, mutations induction and tumor burden assay

$Braf^{CA/+}$; ThyroglobulinCre^{ERT2} single mutant or *$Braf^{CA/+}$; $Pik3ca^{Lat/+}$; ThyroglobulinCre^{ERT2}* double mutant mice from a mixed FVB/C57BL6/F129 background were bred and mutations were induced by daily intraperitoneal injections of 1 mg tamoxifen diluted in peanut oil (100 µL) on five consecutive days. After two months of tumor growth, tumor bearing mice were treated by oral gavage with 30 mg/kg PLX-4720, 50 mg/kg GDC-0941 or the combination of both, or 5 mg/kg PD-0325901 formulated in a solution of 0.5% Hydroxypropylmethylcellulose (HPMC) (Sigma H7509) and 0.2% Tween 80 (Sigma P4780) six days per week. All mice weighed between 20 and 30 g at the start of the experiment. Group allocation for drug treatments was done randomly. Group size was determined using a power calculation assuming the following parameters: difference: 20%; variation: 20%; a 5%; b 50%. Beginning on the first day of drug treatment, tumors were measured by ultrasound measurement every week. For ultrasound measurements mice were anesthetized

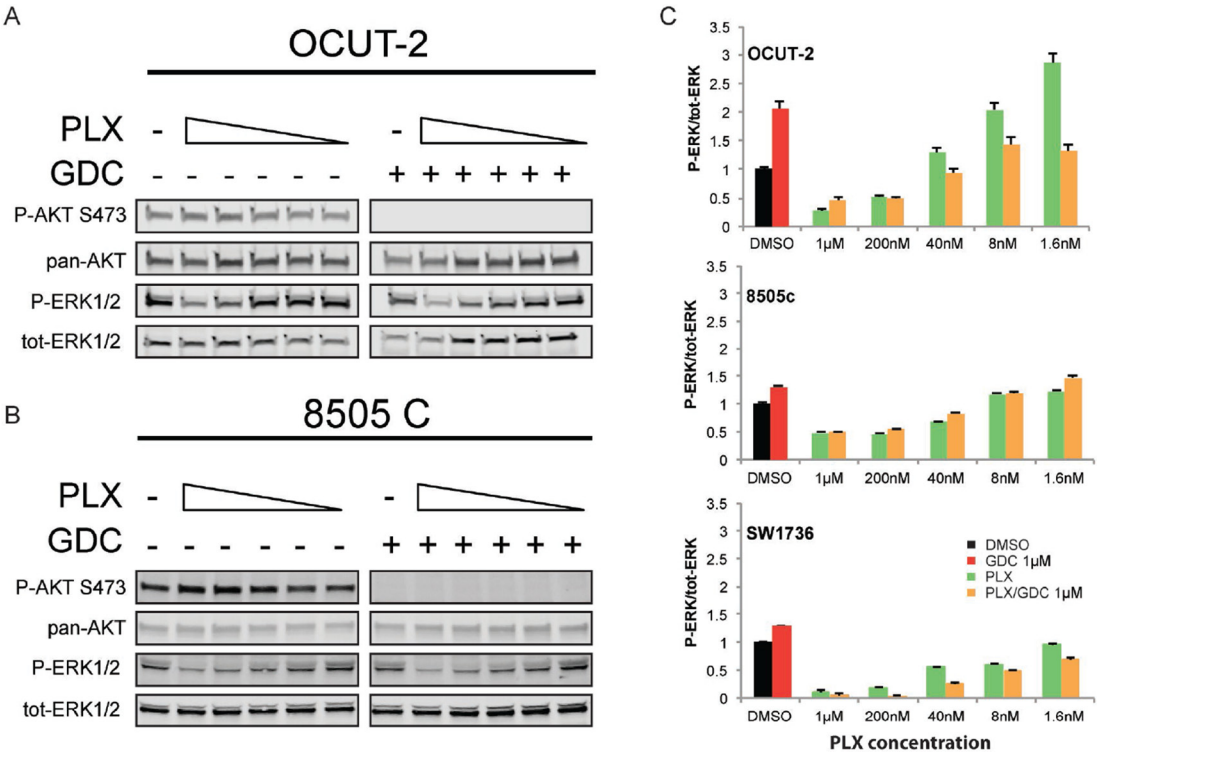

Figure 6: Paradoxical activation of ERK under $BRAF^{V600E}$ specific inhibition treatment is also PI3K-dependent in human ATC cell lines. Representative western blots from total protein extracted from OCUT-2 (**A**) and 8505c (**B**) cells exposed to decreasing concentrations of PLX-4032 (from 1 µM to 1.6 nM) in presence or absence of GDC-0941 at 1 µM. All experiments were performed in triplicate and the quantifications are expressed as average ratios of the three independent experiments (**C**). The western blot of 8505C stands as a representative for both BRAFV600E single mutant cell lines.

using 5 µl/g of body weight of a mixture of 0.1 mg/ml Dorbene, 0.5 mg/ml Dormicum and 5 µg/ml Fentanyl in 0.9% NaCl by intraperitoneal injection. The fur around the neck was epilated with Veet® hair removal cream. Pictures were acquired with an ESAOTE MyLab Five ultrasound machine using a LA455 Probe (18 Mhz) from Siemens. After imaging, mice were taken out of anesthesia with 10 µl/g body weight of a mixture of 0.25 mg/ml Alzan, 5 µg/ml Flumazenil and 20 µg/ml Naloxon in 0.9% NaCl by subcutaneous injection. Images were analyzed using the ImageJ software. Evaluation of tumor burden was performed by the experimenter by measuring the surface of the biggest cross section in mm^2 and normalized to the starting tumor burden of each mouse for comparison.

Total protein preparation from cells

Cells were washed twice with cold PBS, recovered by scraping, then lysed in triton lysis buffer (150 mM NaCl, 50 mM Tris-HCl pH 7.4, 1 mM EDTA pH 8.0, 1% Triton-X-100) complemented with Halt™ Inhibitor Cocktail 1:100 (Pierce, ThermoFischier Scientific). The lysates were incubated 30 min on ice and then cleared by 15 min of centrifugation at 16,000 g at 4 °C. Protein concentrations were quantified by the BCA method (BCA

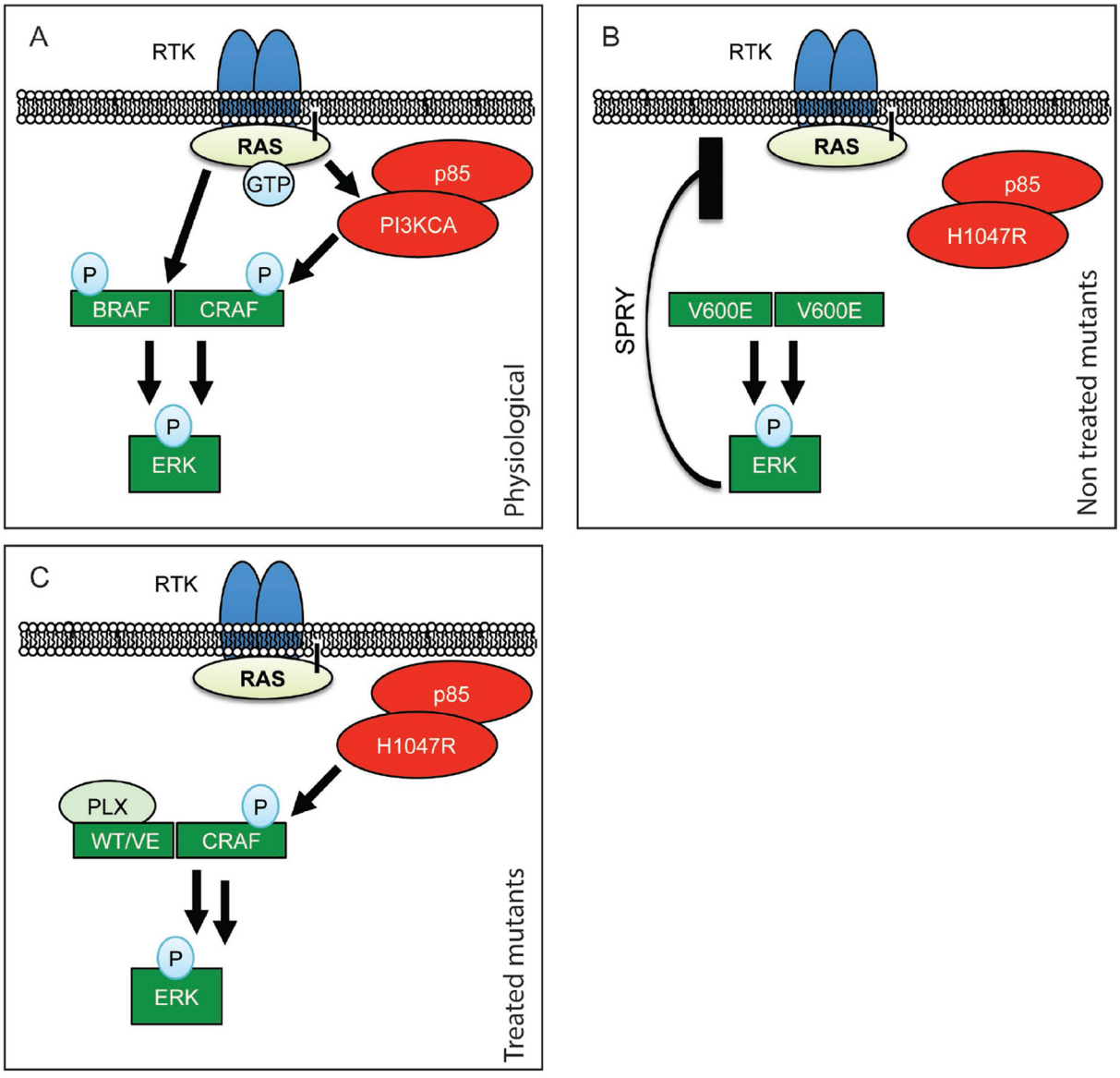

Figure 7: Schematic representation of RAF paradoxical activation. (**A**) In physiological conditions, upon Receptor Tyrosine Kinase (RTK) activation, receptor clustering induces RAS recruitment to the membrane. This results in dimerization of B/CRAF and subsequent phosphorylation that, in fine, induces ERK phosphorylation. (**B**) When BRAF is mutated to $BRAF^{V600E}$ it is able to dimerize without RAS recruitment and induce ERK activation independently from upstream signals. ERK activation results in Sprouty's up-regulation (SPRY) and therefore moderation of the pathway. (**C**) When treated with PLX-4720, $BRAF^{V600E}$ is stabilized in a form that allows its dimerization with CRAF. This complex is then further stimulated by hyperactive PI3'K, leading to paradoxical ERK activation.

Protein Assay Kit, Pierce, ThermoFischer Scientific). Lysates were prepared at 1-4 µg/µl in sample buffer (0.294 M sucrose, 2% SDS, 1 mM EDTA, 60 mM Tris pH 8.8, 0.05% Bromophenol blue, and 26 mM dithiothreitol) and the proteins analyzed by western blotting (see below).

Total protein preparation from mice

Tissues were resected from anesthetized mice (10 mg/ml of Ketamin and 1.6 mg/ml Xylazin, at a dose of 10 µl/g body weight by intraperitoneal injection). After resection, the tissues were washed in ice-cold PBS (137 mM NaCl; 2.7 mM KCl; 18mM KH_2PO_4; 100mMNa_2HPO_4), snap frozen in liquid nitrogen and stored at -80°C until protein extraction. Proteins were extracted from tissue using RIPA buffer (20 mM Tris-base pH 8.0, 150 mM NaCl, 1% Triton-X-100, 0.1% SDS, 0.5% deoxycholate Na+). Halt™ Inhibitor Cocktail was added to the RIPA buffer to prevent dephosphorylation and protein degradation. 100 µl of RIPA plus Halt was added to the tissue samples for lysis using a QIAGEN TissueLyser LT at 50 Hz until complete homogenization (1–2 min). For large pieces of tissue, the amount of lysis buffer was increased. After complete tissue disruption, the sample was incubated on ice for 30 min and then centrifuged for 30 min at 4°C and 17,000 g. Protein concentration of the supernatant was evaluated as described above. All animals were euthanized 4 hours after their last drug administration.

Western blotting

Protein extracts were either loaded separately (for quantifications) or pooled (for figure pictures) for each treatment condition. Proteins were run on TGX precast 4-20% gels (BioRad, Switzerland), transferred onto Trans-Blot transfer pack nitrocellulose (BioRad, Switzerland). Western blots were probed with the following antibodies and concentrations: Primary antibodies (dilution and catalogue number) from Cell Signaling (Purchased from Bioconcept AG, Switzerland): ERK1/2 (1:5000 9107); P-ERK1/2 (1:2000 4370); pan-AKT (1:2000 4691); pan-Akt (1:2000 6040); P-AKT-Ser473 (1:2000 4060) and b-actin (1:5000 or 1:10'000 A2066). Secondary antibodies, Li-Cor Biosciences (Bad Homburg Germany): IRDye 680RD Goat anti-Mouse IgG (H + L) (1:10'000, 926-68071), IRDye 800CW Goat anti-Rabbit IgG (H + L) (1:10'000, 926-32210). Blots were scanned using a Li-Cor ODYSSEY Sa fluorescent western blot scanner and quantified with the ODYSSEY Image Studio software.

Immunofluorescence

Tissue samples for histology were recovered concomitantly to those recovered for proteins, washed in cold PBS and fixed overnight in a neutrally buffered 10% formalin solution (Sigma HT501128). Paraffin-embedded tissue was sectioned to 5 µm. The sections were rehydrated after paraffin removal and targets were retrieved in Tris (Sigma T1503) 10 mM, EGTA (Sigma E4378) 0.5 mM pH = 8.0 solution. The sections were blocked three times for 10 minutes in a buffer of 1% BSA, 0.2% gelatin, and 0.05% Saponin (Sigma 47036) in PBS. The primary antibody KI67 (1:300; Abcam, ab16667) was diluted in 0.1% BSA and 0.3% Triton X-100 in PBS. Other primary antibodies were Ck-19 (1:300; DSHB, 5605s), galectin 3 (1:300 Abcam ab53082), vimentin (1:300 Bioconcept 5741S) and P-ERK1/2 (1:300 Bioconcept 4370L) Primary antibodies were incubated overnight at 4 °C. The slides were then washed three times with 0.1% BSA, 0.2% gelatin and 0.05% Saponin in PBS. The secondary antibody was goat anti-rabbit 488 (Life Technologies A-11034 1:500) complemented by DAPI (Sigma 32670) at 5 µg/ml to counterstain nuclei and incubated for 1 hour at room temperature. Slides were scanned with a Panoramic Midi Scanner (Sysmex/3DHISTECH Switzerland/Hungary). Analysis and quantification was performed on whole tumor sections with the Quant Center software (Sysmex/3DHISTECH Switzerland/Hungary).

Hematoxylin-Eosin Staining

For histological analysis, tissue samples were processed as described above and stained with Hematoxylin (Sigma GHS132) and Eosin (HT110132) following standard protocols.

TUNEL

For TUNEL staining tissue was processed and sectioned according to the procedure described in the preparation of Immunofluorescence slides. Rehydration was also done as described in the Immunofluorescence section. Sections were pretreated with proteinase K (Sigma P2308) with an activity of 0.6 units/ml for 10-20 min in a humidifying chamber at 37°C before they were left to cool at room temperature for 10 min. Subsequently, sections were washed twice in PBS 1x Tween20 (Sigma P9416) 0.1% for 2 min each. To decrease background signal, endogenous biotin was blocked using a kit from Thermo Fisher (E21390). Then sections were pre-incubated in TdT reaction buffer containing 25 mM TRIS-HCl pH 6.6 (Sigma T1503), 200 nM Sodium Cacodylate (Sigma C0250), 0.25 mg/ml BSA and 1 mM Cobalt Chloride (Sigma C8661) for 10 minutes at room temperature. After pre-incubation, the sections were incubated in TdT reaction mixture for 1–2 h at 37°C in a humidifying chamber. TdT reaction mixture contains Terminal deoxynucleutidyl Transferase (TdT) (Sigma 3333566001) and Biotin 16-dUTP (Roche 11093070910). The reaction was stopped by incubating the sections with a buffer containing 300 mM NaCl (Sigma S9888) and 30 mM sodium citrate (Sigma S4641) for 10 min at room temperature. The sections

were then washed three times for 2 min in PBS containing 0.1% Tween20. Before labeling, the slides were blocked with a solution of 3% BSA (Sigma A7906) in PBS 1x, followed by three washing steps (2 min each) with PBS + Tween20 (0.1%). For detection, slides were incubated with a solution containing streptavidin-Alexa Fluor 633 (1:2000 S21375 from LuBioScience) and DAPI 5 µg/ml (32670 Sigma Aldrich). Slides were rinsed with PBS 1x and coverslips were mounted using anti-fading fluorescent mounting medium from DAKO (S3023).

Masson's Trichrome

For Masson's Trichrome staining, tissue was processed and sectioned according to the procedure described in the preparation of Immunofluorescence slides. Rehydration was also done as described in the Immunofluorescence section. Following rehydration slides were incubated with Bouins fixative solution containing 75% saturated picric acid (Sigma P6744), 25% of 37% formaldehyde solution (Sigma 252549) and 5% acetic acid (Sigma 33209) at room temperature overnight. After fixation nuclei were stained with Weigert's hematoxylin solution containing 0.5% hematoxylin (Sigma H9627), 0.5% concentrated HCl (Sigma 320331), 2% of a 29% ferric chloride solution (diluted from 45%) (Sigma 12322), and 47.5% (diluted from 100%) ethanol (Sigma 02860) in distilled water for 10 min at room temperature. Slides were then rinsed under warm running tap water for 10 min, before they were rinsed in distilled water. The extra-nuclear tissue was then stained with the Biebrich Scarlet- Acid Fuchsin solution containing 89% of a 1% Biebrich Scarlet solution (Sigma B6008), 10% of a 1% Acid Fuchsin (Sigma F8129) solution and 1% of acetic acid for 10 min at room temperature, followed by rinsing in distilled water until clear. To remove the stain from the collagen for differentiation, the slides were subsequently incubated with a solution containing 50% of a 5% phosphomolybdic acid solution (Sigma HT153) and 50% of a 5% phosphotungstic acid solution (Sigma HT152) for 10 min at room temperature. Then slides were transferred to a solution containing 2.5% Aniline Blue (Sigma 415049) and 2% acetic acid in distilled water for 10 min at room temperature for counterstaining of collagen. Slides were then dehydrated rapidly in a succession of two baths of 1% acetic acid followed by 1 bath of 95% ethanol and two baths of 100% ethanol. Slides were then left in a xylene bath until mounting in Eukitt® Quick-hardening mounting medium (Sigma 03989).

Statistical methods

All statistical analyses were performed in GraphPad®. Tumor growth experiments were analyzed using the Mann-Whitney test to compare the groups. The remaining experiments were analyzed using one-way ANOVA with a Fisher's exact test for post hoc testing. In cases where there were only two groups to compare, a two-tailed t-Test was used. Significance is displayed using stars with one star meaning a resulting *p*-value of smaller than or equal to 0.05. Two stars means a *p*-value of smaller than or equal to 0.01. Three stars stands for a *p*-value of smaller than or equal to 0.001. If a *p*-value was greater than 0.05 the difference between the two concerned groups was regarded as not significant.

Ethics approval

Mice were kept, treated and euthanized according to the Swiss federal guidelines. The experimental protocol was approved by the Bernese cantonal ethical commission for animal experimentation (License number: BE120/13).

Author contributions

In vivo experiments: MAR and OEM; *In vitro* experiments: DRD; Tissue staining: MAR and AS; Wester slots: MAR; Data analysis: MAR; Animal breeding, genotyping: AS and MAR; Histopathological analysis: MSD; Manuscript writing: RPC, MAR, DRD, MSD and WAP; Figure preparation: MAR, DRD, RPC; Design: RPC; Study supervision: RPC.

ACKNOWLEDGMENTS

Special thanks to Prof. Martin McMahon for his former support, mentoring and for the *Braf*^{CA} mice. Further, special thanks to Prof. Engelhard, Dr. Deutsch and Dr. Benarafa for allowing us to keep our mice in the vivarium at the Theodor Kocher Institute. Finally, to Prof. Dimitrios Fotiadis for his pushes in the right direction. Also, we would like to acknowledge the Microscopy Imaging center (MIC) of the University of Bern. Mr Roelli and Mr ElMokh are enrolled in the Graduate School for Cellular and Biomedical Sciences (GCB) of the University of Bern, that we would like to acknowledge for the training provided.

CONFLICTS OF INTEREST

The author declare that they have no competing interests.

FUNDING

This work was supported by the Swiss National Science Foundation grant 31003A_149824/1. The RPC lab is also supported by the Swiss National Science Foundation grant NCCR-TransCure. WAP is supported, in part, by project grant APP1080491 from the National Health and Medical Research Council (NHMRC) of Australia.

REFERENCES

1. Quiros RM, Ding HG, Gattuso P, Prinz RA, Xu X. Evidence that one subset of anaplastic thyroid carcinomas are derived from papillary carcinomas due to BRAF and p53 mutations. Cancer. 2005; 103:2261–8. https://doi.org/10.1002/cncr.21073.
2. Nagaiah G, Hossain A, Mooney CJ, Parmentier J, Remick SC, Nagaiah G, Hossain A, Mooney CJ, Parmentier J, Remick SC. Anaplastic Thyroid Cancer: A Review of Epidemiology, Pathogenesis, and Treatment. J Oncol. 2011; 2011:1–13. https://doi.org/10.1155/2011/542358.
3. McIver B, Hay ID, Giuffrida DF, Dvorak CE, Grant CS, Thompson GB, Van Heerden JA, Goellner JR. Anaplastic thyroid carcinoma: A 50-year experience at a single institution. Surgery. 2001; 130:1028–34. https://doi.org/10.1067/msy.2001.118266.
4. Perri F, Lorenzo GD, Scarpati GD, Buonerba C. Anaplastic thyroid carcinoma: A comprehensive review of current and future therapeutic options plastic thyroid carcinoma: A comprehensive review of current and future therapeutic options. World J Clin Oncol. 2011; 2:150–7. https://doi.org/10.5306/wjco.v2.i3.150.
5. Xing M. Molecular pathogenesis and mechanisms of thyroid cancer. Nat Rev Cancer. 2013; 13:184–99. https://doi.org/10.1038/nrc3431.
6. Nikiforov YE, Nikiforova MN. Molecular genetics and diagnosis of thyroid cancer. Nat Rev Endocrinol. 2011; 7:569–80. https://doi.org/10.1038/nrendo.2011.142.
7. Charles RP, Iezza G, Amendola E, Dankort D, McMahon M. Mutationally activated BRAFV600E elicits papillary thyroid cancer in the adult mouse. Cancer Res. 2011; 71:3863–71. https://doi.org/10.1158/0008-5472.CAN-10-4463.
8. Knauf JA, Ma X, Smith EP, Zhang L, Mitsutake N, Liao XH, Refetoff S, Nikiforov YE, Fagin JA. Targeted Expression of BRAFV600E in Thyroid Cells of Transgenic Mice Results in Papillary Thyroid Cancers that Undergo Dedifferentiation. Cancer Res. 2005; 65:4238–45. https://doi.org/10.1158/0008-5472.CAN-05-0047.
9. McFadden DG, Vernon A, Santiago PM, Martinez-McFaline R, Bhutkar A, Crowley DM, McMahon M, Sadow PM, Jacks T. p53 constrains progression to anaplastic thyroid carcinoma in a Braf-mutant mouse model of papillary thyroid cancer. Proc Natl Acad Sci. 2014; 111:E1600–9. https://doi.org/10.1073/pnas.1404357111.
10. Charles RP, Silva J, Iezza G, Phillips WA, McMahon M. Activating BRAF, PIK3CA Mutations Cooperate to Promote Anaplastic Thyroid Carcinogenesis. Mol Cancer Res. 2014; 12:979–86. https://doi.org/10.1158/1541-7786.MCR-14-0158-T.
11. Okkenhaug K. Signaling by the phosphoinositide 3-kinase family in immune cells. Annu Rev Immunol. 2013; 31:675–704. https://doi.org/10.1146/annurev-immunol-032712-095946.
12. Vivanco I, Sawyers CL. The phosphatidylinositol 3-Kinase–AKT pathway in human cancer. Nat Rev Cancer. 2002; 2:489–501. https://doi.org/10.1038/nrc839.
13. Fruman DA, Rommel C. PI3K and cancer: lessons, challenges and opportunities. Nat Rev Drug Discov. 2014; 13:140–56. https://doi.org/10.1038/nrd4204.
14. Samuels Y, Wang Z, Bardelli A, Silliman N, Ptak J, Szabo S, Yan H, Gazdar A, Powel S, Riggins G, Willson J, Markowitz S, Kinzler K, et al. High frequency of mutations of the PIK3Ca gene in human cancers. Science (80-). 2004; 304:554. https://doi.org/10.1126/science.1096502.
15. García-Rostán G, Costa AM, Pereira-Castro I, Salvatore G, Hernandez R, Hermsem MJ, Herrero A, Fusco A, Cameselle-Teijeiro J, Santoro M. Mutation of the PIK3CA gene in anaplastic thyroid cancer. Cancer Res. 2005; 65:10199–207. https://doi.org/10.1158/0008-5472.CAN-04-4259.
16. Liu D, Mambo E, Ladenson PW, Xing M. Letter re: Uncommon Mutation but Common Amplifications of the PIK3CA Gene in Thyroid Tumors. J Clin Endocrinol Metab. 2005; 90:5509–5509. https://doi.org/10.1210/jc.2005-1726.
17. Bollag G, Hirth P, Tsai J, Zhang J, Ibrahim PN, Cho H, Spevak W, Zhang C, Zhang Y, Habets G, Burton EA, Wong B, Tsang G, et al. Clinical efficacy of a RAF inhibitor needs broad target blockade in BRAF-mutant melanoma. Nature. 2010; 467:596–9. https://doi.org/10.1038/nature09454.
18. Chapman PB, Hauschild A, Robert C, Haanen JB, Ascierto P, Larkin J, Dummer R, Garbe C, Testori A, Maio M, Hogg D, Lorigan P, Lebbe C, et al. Improved Survival with Vemurafenib in Melanoma with BRAF V600E Mutation. N Engl J Med. 2011; 364:2507–16. https://doi.org/10.1056/NEJMoa1103782.
19. Flaherty KT, Puzanov I, Kim KB, Ribas A, McArthur GA, Sosman JA, O'Dwyer PJ, Lee RJ, Grippo JF, Nolop K, Chapman PB. Inhibition of Mutated, Activated BRAF in Metastatic Melanoma. N Engl J Med. 2010; 363:809–19. https://doi.org/10.1056/NEJMoa1002011.
20. Montagut C, Sharma SV, Shioda T, McDermott U, Ulman M, Ulkus LE, Dias-Santagata D, Stubbs H, Lee DY, Singh A, Drew L, Haber DA, Settleman J. Elevated CRAF as a potential mechanism of acquired resistance to BRAF inhibition in melanoma. Cancer Res. 2008; 68:4853–61. https://doi.org/10.1158/0008-5472.CAN-07-6787.
21. Poulikakos PI, Persaud Y, Janakiraman M, Kong X, Ng C, Moriceau G, Shi H, Atefi M, Titz B, Gabay MT, Salton M, Dahlman KB, Tadi M, et al. RAF inhibitor resistance is mediated by dimerization of aberrantly spliced BRAF(V600E). Nature. 2011; 480:387–90. https://doi.org/10.1038/nature10662.
22. Corcoran RB, Dias-Santagata D, Bergethon K, Iafrate AJ, Settleman J, Engelman JA. BRAF gene amplification can promote acquired resistance to MEK inhibitors in cancer cells harboring the BRAF V600E mutation. Sci Signal. 2010; 3:ra84. https://doi.org/10.1126/scisignal.2001148.
23. Shi H, Moriceau G, Kong X, Lee MK, Lee H, Koya RC, Ng C, Chodon T, Scolyer RA, Dahlman KB, Sosman JA,

Kefford RF, Long GV, et al. Melanoma whole-exome sequencing identifies (V600E)B-RAF amplification-mediated acquired B-RAF inhibitor resistance. Nat Commun. 2012; 3:724. https://doi.org/10.1038/ncomms1727.

24. Nazarian R, Shi H, Wang Q, Kong X, Koya RC, Lee H, Chen Z, Lee MK, Attar N, Sazegar H, Chodon T, Nelson SF, McArthur G, et al. Melanomas acquire resistance to B-RAF(V600E) inhibition by RTK or N-RAS upregulation. Nature. 2010; 468:973–7. https://doi.org/10.1038/nature09626.

25. Wagle N, Emery C, Berger MF, Davis MJ, Sawyer A, Pochanard P, Kehoe SM, Johannessen CM, MacConaill LE, Hahn WC, Meyerson M, Garraway LA. Dissecting therapeutic resistance to RAF inhibition in melanoma by tumor genomic profiling. J Clin Oncol. 2011; 29:3085–96. https://doi.org/10.1200/JCO.2010.33.2312.

26. Rosove MH, Peddi PF, Glaspy JA. BRAF V600E Inhibition in Anaplastic Thyroid Cancer. N Engl J Med. 2013; 368:684–5. https://doi.org/10.1056/NEJMc1214556.

27. Marten KA, Gudena VK. Use of vemurafenib in anaplastic thyroid carcinoma: a case report. Cancer Biol Ther. 2015; 16:1430–3. https://doi.org/10.1080/15384047.2015.1071734.

28. Kim KB, Cabanillas ME, Lazar AJ, Williams MD, Sanders DL, Ilagan JL, Nolop K, Lee RJ, Sherman SI. Clinical responses to vemurafenib in patients with metastatic papillary thyroid cancer harboring BRAF(V600E) mutation. Thyroid. 2013; 23:1277–83. https://doi.org/10.1089/thy.2013.0057.

29. Hyman DM, Puzanov I, Subbiah V, Faris JE, Chau I, Blay JY, Wolf J, Raje NS, Diamond EL, Hollebecque A, Gervais R, Elez-Fernandez ME, Italiano A, et al. Vemurafenib in Multiple Nonmelanoma Cancers with BRAF V600 Mutations. N Engl J Med. 2015; 373:726–36. https://doi.org/10.1056/NEJMoa1502309.

30. Lito P, Pratilas CA, Joseph EW, Tadi M, Halilovic E, Zubrowski M, Huang A, Wong WL, Callahan MK, Merghoub T, Wolchok JD, de Stanchina E, Chandarlapaty S, et al. Relief of Profound Feedback Inhibition of Mitogenic Signaling by RAF Inhibitors Attenuates Their Activity in BRAFV600E Melanomas. Cancer Cell. 2012; 22:668–82. https://doi.org/10.1016/j.ccr.2012.10.009.

31. Hight MR, Cheung YY, Nickels ML, Dawson ES, Zhao P, Saleh S, Buck JR, Tang D, Washington MK, Coffey RJ, Manning HC. A peptide-based positron emission tomography probe for *in vivo* detection of caspase activity in apoptotic cells. Clin Cancer Res. 2014; 20:2126–35. https://doi.org/10.1158/1078-0432.CCR-13-2444.

32. Perna D, Karreth FA, Rust AG, Perez-Mancera PA, Rashid M, Iorio F, Alifrangis C, Arends MJ, Bosenberg MW, Bollag G, Tuveson DA, Adams DJ. BRAF inhibitor resistance mediated by the AKT pathway in an oncogenic BRAF mouse melanoma model. Proc Natl Acad Sci U S A. 2015; 112:E536-45. https://doi.org/10.1073/pnas.1418163112.

33. Shah N, Iyer RM, Mair HJ, Choi DS, Tian H, Diodone R, Fähnrich K, Pabst-Ravot A, Tang K, Scheubel E, Grippo JF, Moreira SA, Go Z, et al. Improved human bioavailability of vemurafenib, a practically insoluble drug, using an amorphous polymer-stabilized solid dispersion prepared by a solvent-controlled coprecipitation process. J Pharm Sci. 2013; 102:967–81. https://doi.org/10.1002/jps.23425.

34. Barrett SD, Bridges AJ, Dudley DT, Saltiel AR, Fergus JH, Flamme CM, Delaney AM, Kaufman M, LePage S, Leopold WR, Przybranowski SA, Sebolt-Leopold J, Van Becelaere K, et al. The discovery of the benzhydroxamate MEK inhibitors CI-1040 and PD 0325901. Bioorganic Med Chem Lett. 2008; 18:6501–4. https://doi.org/10.1016/j.bmcl.2008.10.054.

35. Elmokh O, Ruffieux-Daidié D, Roelli MA, Stooss A, Phillips WA, Gertsch J, Dettmer MS, Charles R. Combined MEK and Pi3 ' -kinase inhibition reveals synergy in targeting thyroid cancer *in vitro* and *in vivo*. Oncotarget. 2017; 8:24604–20. https://doi.org/10.18632/oncotarget.15599.

36. Holderfield M, Deuker MM, McCormick F, McMahon M. Targeting RAF kinases for cancer therapy: BRAF-mutated melanoma and beyond. Nat Rev Cancer. 2014; 14:455–67. https://doi.org/10.1038/nrc3760.

37. Davies H, Bignell GR, Cox C, Stephens P, Edkins S, Clegg S, Teague J, Woffendin H, Garnett MJ, Bottomley W, Davis N, Dicks E, Ewing R, et al. Mutations of the BRAF gene in human cancer. Nature. 2002; 417:949–54. https://doi.org/10.1038/nature00766.

38. Xing M. BRAF mutation in thyroid cancer. Endocr Relat Cancer. 2005; 12:245–62. https://doi.org/10.1677/erc.1.0978.

39. Mao M, Tian F, Mariadason JM, Tsao CC, Lemos R, Dayyani F, Vashisht Gopal YN, Jiang ZQ, Wistuba II, Tang XM, Bornman WG, Bollag G, Mills GB, et al. Resistance to BRAF inhibition in BRAF-mutant colon cancer can be overcome with PI3K inhibition or demethylating agents. Clin Cancer Res. 2013; 19:657–67. https://doi.org/10.1158/1078-0432.CCR-11-1446.

40. Faes S, Dormond O. PI3K, AKT: Unfaithful partners in cancer. Int J Mol Sci. 2015; 16:21138–52. https://doi.org/10.3390/ijms160921138.

41. Holderfield M, Nagel TE, Stuart DD. Mechanism and consequences of RAF kinase activation by small-molecule inhibitors. Br J Cancer. 2014; 111:640–5. https://doi.org/10.1038/bjc.2014.139.

42. Su F, Viros A, Milagre C, Trunzer K, Bollag G, Spleiss O, Reis-Filho JS, Kong X, Koya RC, Flaherty KT, Chapman PB, Kim MJ, Hayward R, et al. RAS mutations in cutaneous squamous-cell carcinomas in patients treated with BRAF inhibitors. N Engl J Med. 2012; 366:207–15. https://doi.org/10.1056/NEJMoa1105358.

43. Hatzivassiliou G, Song K, Yen I, Brandhuber BJ, Anderson DJ, Alvarado R, Ludlam MJC, Stokoe D, Gloor SL, Vigers

G, Morales T, Aliagas I, Liu B, et al. RAF inhibitors prime wild-type RAF to activate the MAPK pathway and enhance growth. Nature. 2010; 464:431–5. https://doi.org/10.1038/nature08833.

44. Boussemart L, Girault I, Malka-Mahieu H, Mateus C, Routier E, Rubington M, Kamsu-Kom N, Thomas M, Tomasic G, Agoussi S, Breckler M, Laporte M, Lacroix L, et al. Secondary tumors arising in patients undergoing BRAF inhibitor therapy exhibit increased BRAF-CRAF heterodimerization. Cancer Res. 2016; 76:1476–84. https://doi.org/10.1158/0008-5472.CAN-15-2900-T.

45. Chatelle CV, Hövermann D, Müller A, Wagner HJ, Weber W, Radziwill G. Optogenetically controlled RAF to characterize BRAF and CRAF protein kinase inhibitors. Sci Rep. 2016; 6. https://doi.org/10.1038/srep23713.

46. Karoulia Z, Wu Y, Ahmed TA, Xin Q, Bollard J, Krepler C, Wu X, Zhang C, Bollag G, Herlyn M, Fagin JA, Lujambio A, Gavathiotis E, et al. An Integrated Model of RAF Inhibitor Action Predicts Inhibitor Activity against Oncogenic BRAF Signaling. Cancer Cell. 2016; 30:485–98. https://doi.org/10.1016/j.ccell.2016.06.024.

47. Escuin-Ordinas H, Li S, Xie MW, Sun L, Hugo W, Huang RR, Jiao J, Meira De-Faria F, Realegeno S, Krystofinski P, Azhdam A, Marie S, Komenan D, et al. ARTICLE Cutaneous wound healing through paradoxical MAPK activation by BRAF inhibitors. Nat Commun. 2016; 7. https://doi.org/10.1038/ncomms12348.

48. Chaudhary A, King WG, Mattaliano MD, Frost JA, Diaz B, Morrison DK, Cobb MH, Marshall MS, Brugge JS. Phosphatidylinositol 3-kinase rgulates Raf1 through Pak phosphorylation of serine 338. Curr Biol. 2000; 10:551–4.

49. Nehs MA, Nucera C, Nagarkatti SS, Sadow PM, Morales-Garcia D, Hodin RA, Parangi S. Late Intervention with anti-BRAFV600E Therapy Induces Tumor Regression in an Orthotopic Mouse Model of Human Anaplastic Thyroid Cancer. Endocrinology. 2011; 153:985–94. https://doi.org/10.1210/en.2011-1519.

50. Le Scodan R, Mornex F, Partensky C, Mercier C, Valette PJ, Ychou M, Roy P, Scoazec JY. Histopathological response to preoperative chemoradiation for resectable pancreatic adenocarcinoma: the French Phase II FFCD 9704-SFRO Trial. Am J Clin Oncol. 2008; 31:545–52. https://doi.org/10.1097/COC.0b013e318172d5c5.

51. Dworak O, Keilholz L, Hoffmann A. Pathological features of rectal cancer after preoperative radiochemotherapy. Int J Colorectal Dis. 1997; 12:19–23. https://doi.org/10.1007/s003840050072.

52. Pefiot JF, Roussel A, Jacob JH, Segol P, Samama G, Ollivier JM, Bonvalot S, Gignoux M. Pathologic Assessment of Tumor Regression after Preoperative Chemoradiotherapy of Esophageal Carcinoma Clinicopa thologic Correlations. Cancer. 1994; 73:2680–6.

53. Edin ML, Juliano RL. Raf-1 Serine 338 Phosphorylation Plays a Key Role in Adhesion-Dependent Activation of Extracellular Signal-Regulated Kinase by Epidermal Growth Factor Raf-1 Serine 338 Phosphorylation Plays a Key Role in Adhesion-Dependent Activation of Extracellular Sign. Mol Cell Biol. 2005; 25:4466–75. https://doi.org/10.1128/MCB.25.11.4466.

54. Montero-Conde C, Ruiz-Llorente S, Dominguez JM, Knauf JA, Viale A, Sherman EJ, Ryder M, Ghossein RA, Rosen N, Fagin JA. Relief of feedback inhibition of HER3 transcription by RAF and MEK inhibitors attenuates their antitumor effects in BRAF -mutant thyroid carcinomas. Cancer Discov. 2013; 3:520–33. https://doi.org/10.1158/2159-8290.CD-12-0531.

55. Nagarajah J, Le M, Knauf JA, Ferrandino G, Montero-Conde C, Pillarsetty N, Bolaender A, Irwin C, Krishnamoorthy GP, Saqcena M, Larson SM, Ho AL, Seshan V, et al. Sustained ERK inhibition maximizes responses of BrafV600E thyroid cancers to radioiodine. J Clin Invest. 2016; 126:4119–24. https://doi.org/10.1172/JCI89067.

56. Simeone E, Grimaldi AM, Festino L, Vanella V, Palla M, Ascierto PA. Combination Treatment of Patients with BRAF-Mutant Melanoma: A New Standard of Care. BioDrugs. 2017; 31:51–61. https://doi.org/10.1007/s40259-016-0208-z.

57. Das Thakur M, Salangsang F, Landman AS, Sellers WR, Pryer NK, Levesque MP, Dummer R, McMahon M, Stuart DD. Modelling vemurafenib resistance in melanoma reveals a strategy to forestall drug resistance. Nature. 2013; 494:251–5. https://doi.org/10.1038/nature11814.

58. Zhang C, Spevak W, Zhang Y, Burton EA, Ma Y, Habets G, Zhang J, Lin J, Ewing T, Matusow B, Tsang G, Marimuthu A, Cho H, et al. RAF inhibitors that evade paradoxical MAPK pathway activation. Nature. 2015; 526:583–6. https://doi.org/10.1038/nature14982.

59. Nobuhara Y, Onoda N, Yamashita Y, Yamasaki M, Ogisawa K, Takashima T, Ishikawa T, Hirakawa K. Efficacy of epidermal growth factor receptor-targeted molecular therapy in anaplastic thyroid cancer cell lines. Br J Cancer. 2005; 92:1110–6. https://doi.org/10.1038/sj.bjc.6602461.